Scientific Research Publishing

Applied Mathematics, 2025, 16(8), 637-656
https://www.scirp.org/journal/am
ISSN Online: 2152-7393
ISSN Print: 2152-7385

Two Parameters Lie Group Analysis for the Effect of Brownian Diffusion on Viscoelastic Nanofluid Flow in a Channel with Convective Wall

M. Enamul Karim[1], M. Abdus Samad[2]

[1]Department of Mathematics, Comilla University, Cumilla, Bangladesh
[2]Department of Applied Mathematics, University of Dhaka, Dhaka, Bangladesh
Email: ekarim777@gmail.com, ekarim@cou.ac.bd, samad@du.ac.bd

How to cite this paper: Karim, M.E. and Samad, M. A. (2025) Two Parameters Lie Group Analysis for the Effect of Brownian Diffusion on Viscoelastic Nanofluid Flow in a Channel with Convective Wall. *Applied Mathematics*, **16**, 637-656.
https://doi.org/10.4236/am.2025.168035

Received: July 12, 2025
Accepted: August 19, 2025
Published: August 22, 2025

Abstract

The current research investigates the heat transfer phenomena of the time-dependent viscoelastic nanofluid stream in a parallel plate channel of a convective stretching wall. The Lie group theory transforms the recent physical configuration into a nonlinear differential system. This scheme is numerically decrypted with the collocation method. The outcomes of several flow controllers are investigated for the motion, energy, and mass diffusion distributions. The impacts of skin friction and the Nusselt number, considering two scenarios, prescribed convective boundary (PCB) and prescribed surface temperature (PST), have been described. And the consequences of the study are illustrated from a substantial point of view. Generally, the PST and PCB peripheral circumstances are very serviceable in automobile engineering appliances. Furthermore, a remarkable consequence of the current investigation is that the nanofluid viscosity enhances with the ongoing growth in the Deborah number, which improves the resistance to motion. And a crosswise flow exists in the channel adjacent to the extending wall.

Keywords

Convective Surface, Deborah Number, Elastico-Viscous Fluid, Lie Group Theory, Nanofluid

1. Introduction

Nanofluid is an innovatively engineered heat transfer fluid that exhibits enhanced thermal conductivity at lower particle concentrations compared to conventional

fluids. It is made by stably suspending and uniformly dispersing a few metallic or nonmetallic particles in ordinary heat transfer fluids. These particles are ultrafine and nano-scaled. Choi [1] developed the idea of nanofluid in 1995. Recent researchers have revealed that swapping traditional fluids with artificial nanofluids can be advantageous in enhancing the heat transfer performance in nuclear and engineering applications and cooling down automobile appliances [2]-[8]. Buongiorno [9] established a scientific model to explore heat transfer by convection in nanofluids. This model incorporates two crucial factors, namely Brownian and thermophoretic transmissions. Zangooee *et al.* [10] investigated the nanoparticle addition effects on the water flowing between two rotating plates using the Akbari-Ganji Method. They chose different nanoparticles which can enhance water's thermodynamic and thermal properties. Seadawy *et al.* [11] clarified the analytical and mathematical dimensions of nanofluids having practical uses in mechanical devices. Rashidi *et al.* [12] analysed the entropy generation ratio in nanofluid drift concerning clutching disks.

Furthermore, the mutual effect of conductive fluids and electromagnetic fields represents magneto-hydrodynamics (MHD). Various purposes of nanofluids originated in industrial and engineering premises, primarily in the heat conversation devices design, accelerators, MHD generators, etc. [13]-[17]. Pavar *et al.* [18] discussed the convective MHD flow carried over a permeable exponentially prolonging surface, giving importance in clinical and medical research to generate 3D anatomical images from nuclear magnetic resonance signals. Li *et al.* [19] investigated the axisymmetric transient squeezing MHD flow of the Newtonian non-conducting fluid over a porous structure retaining the slip condition at the periphery.

A fascinating and unsettled tribological subject entails the viscoelasticity impact on thin-film flows**.** The preparation of mixing polymers with mineral lubricants has been renowned later the mid-1990s [20]-[22]. These mixtures drive the consequential oils to behave like non-Newtonian fluids by performing a viscosity dependency on the shear rate [23]-[25]. The classic Newtonian prototype covering the Navier-Stokes equations is unable to exhibit the extremely non-linear bondings between tangential stress and strain rate of non-Newtonian lubricants [26]-[30]. Harris [20] established the upper convected Maxwell Fluid (UCM) features to exhibit the lubricant behaviour of a non-Newtonian fluid. Upper convected Maxwell fluid is a regular rate-type viscoelastic material with fluid relaxation time features, namely the viscosity-modulus of elasticity ratio. It rejects the multifaceted properties of shear-related viscosity. It also establishes the effect of fluid elasticity on the physical appearance of its boundary layer [27] [31]. Due to the explosion of concrete applications in bioengineering and plastic manufacturing, paper fabrication, and food processing, investigators have paid attention to studying the boundary layer theory of non-Newtonian lubricant flow [32]-[36].

Lie group transformation scheme is a developing field of mathematics with numerous purposes. Norwegian mathematician Sophus Lie developed a classic Lie

group transformation scheme to discover invariant and similarity solutions [37]-[42]. The Lie group study offers an applicable method to concentrate on nonlinear equations. This method recommends a particular mathematical presentation of observant opinions of symmetry and deals with essential techniques for analysing non-linear differential systems. Investigators are now exploring the transformations of the Lie group for Newtonian and non-Newtonian fluid flows [40] [43]-[45].

However, the Maxwell model enlightens the time-dependent stress relaxation of fluid accommodating substantial nanoparticles; the non-Newtonian Nanofluid with developed heat transfer has countless prospects to influence manufacturing and hemodynamic rationales. Even if the higher heat transfer procedure in non-Newtonian nanofluids is crucial, a study has been performed in this investigation. By perceiving the prior research, the principal attention is to analyse the time-dependent two-dimensional elastico-viscous nanofluid stream in two parallel convective stretched walls incorporating Maxwell's rheological Nanofluid model using the Lie group scheme.

2. Model Equations

An unsteady elastico-viscous nanofluid flow is engaged through two parallel walls to demonstrate the physical configuration. The upper surface is stretched and porous, and the lower has convective boundary conditions. The Cartesian coordinate system is accommodated to explain the physical model. The $\bar{x}$ -axis is occupied along the walls, and the $\bar{y}$ -axis is upright to the walls, as displayed in **Figure 1**.

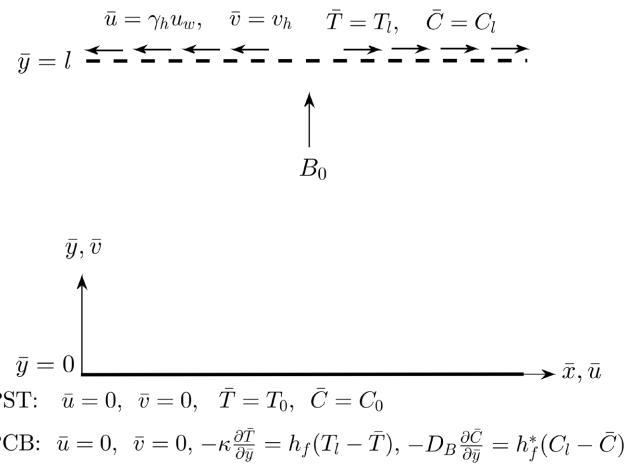

Figure 1. Physical configuration of the model.

The viscoelastic activities of fluid will be observed if elastic stress is applied, and the resultant strain will be contingent upon time, featuring the relaxation phase. The constitutive equation [27] of time-dependent stress relaxation is

$$\tau = -pI + S \tag{1}$$

When an extra stress tensor $\boldsymbol{S}$ is applied, the elastico-viscous behaviour of the nanofluid, demonstrated by the Maxwell model [34], is given by

$$S+\lambda_S\left(\frac{\mathrm{d}S}{\mathrm{d}t}+V\cdot\nabla S-LS-SL^{\mathrm{tr}}\right)=\mu_{nf}\left(L+L^{\mathrm{tr}}\right) \tag{2}$$

Here V means the nanofluid's velocity, $L^{\mathrm{tr}}=\nabla V$ is the velocity gradient, the 'tr' signifies a transpose, $L_{ij}=\frac{\partial u_i}{\partial x_j}$, $\lambda_S>0$ is the stress reduction time of non-Newtonian fluids, and $\lambda_S=0$ provides Newtonian fluids. Then the equations of flow are given by

$$\frac{\partial\overline{u}}{\partial\overline{x}}+\frac{\partial\overline{v}}{\partial\overline{y}}=0 \tag{3}$$

$$\begin{aligned}&\frac{\partial\overline{u}}{\partial\overline{t}}+\overline{u}\frac{\partial\overline{u}}{\partial\overline{x}}+\overline{v}\frac{\partial\overline{u}}{\partial\overline{y}}+\lambda_S\left(\frac{\partial^2\overline{u}}{\partial\overline{t}^2}+2\overline{u}\frac{\partial^2\overline{u}}{\partial\overline{t}\,\partial\overline{x}}+2\overline{v}\frac{\partial^2\overline{u}}{\partial\overline{t}\,\partial\overline{y}}+\overline{u}^2\frac{\partial^2\overline{u}}{\partial\overline{x}^2}+\overline{v}^2\frac{\partial^2\overline{u}}{\partial\overline{y}^2}+2\overline{u}\overline{v}\frac{\partial^2\overline{u}}{\partial\overline{x}\,\partial\overline{y}}\right)\\&=-\frac{1}{\rho}\frac{\partial\overline{p}}{\partial\overline{x}}+\nu\frac{\partial^2\overline{u}}{\partial\overline{y}^2}-\frac{\sigma B_0^2}{\rho}\left(\overline{u}+\lambda_S\left(\frac{\partial\overline{u}}{\partial\overline{t}}+\overline{v}\frac{\partial\overline{u}}{\partial\overline{y}}\right)\right)\end{aligned} \tag{4}$$

Again, considering the Buongiorno model integrating thermophoresis and Brownian diffusion effects [9] [46], the equations of energy and nanoparticle concentration are

$$\begin{aligned}&\frac{\partial\overline{T}}{\partial\overline{t}}+\overline{u}\frac{\partial\overline{T}}{\partial\overline{x}}+\overline{v}\frac{\partial\overline{T}}{\partial\overline{y}}\\&=\frac{\kappa}{\rho c_p}\left(\frac{\partial^2\overline{T}}{\partial\overline{y}^2}\right)+\tau\left(D_B\left(\frac{\partial\overline{T}}{\partial\overline{y}}\frac{\partial\overline{C}}{\partial\overline{y}}\right)+\frac{D_T}{T_a}\left(\frac{\partial\overline{T}}{\partial\overline{y}}\right)^2\right)+\frac{\mu}{\rho c_p}\left(\left(\frac{\partial\overline{u}}{\partial\overline{y}}\right)^2\right)\end{aligned} \tag{5}$$

$$\frac{\partial\overline{C}}{\partial\overline{t}}+\overline{u}\frac{\partial\overline{C}}{\partial\overline{x}}+\overline{v}\frac{\partial\overline{C}}{\partial\overline{y}}=D_B\frac{\partial^2\overline{C}}{\partial\overline{y}^2}+\frac{D_T}{T_a}\frac{\partial^2\overline{T}}{\partial\overline{y}^2} \tag{6}$$

The resolutions of the model differ with the nature of the prescribed thermal boundary condition [32]. The corresponding boundary conditions are:

Case 1: Prescribed surface temperature (PST)

$$\left.\begin{aligned}&\overline{u}=\gamma_h u_w,\ \overline{v}=v_h,\ \ \overline{T}=T_l,\ \overline{C}=C_l \quad \text{at } \overline{y}=l\\&\overline{u}=0,\quad \overline{v}=0,\ \ \overline{T}=\overline{T}_0,\ \overline{C}=\overline{C}_0 \quad \text{at } \overline{y}=0\end{aligned}\right\} \tag{7}$$

Case 2: Prescribed convective boundary (PCB) case

$$\left.\begin{aligned}&\overline{u}=\gamma_h u_w,\ \overline{v}=v_h,\quad \overline{T}=T_l, \qquad\qquad \overline{C}=C_l \qquad \text{at } \overline{y}=l\\&\overline{u}=0,\ \overline{v}=0,\quad -\kappa\frac{\partial\overline{T}}{\partial\overline{y}}=h_f\left(T_l-\overline{T}\right),\ -D_B\frac{\partial\overline{C}}{\partial\overline{y}}=h_f^*\left(C_l-\overline{C}\right) \quad \text{at } \overline{y}=0\end{aligned}\right\} \tag{8}$$

Here $T_l=T_0+\left(T_h-T_0\right)\frac{x}{\left(1-t\right)^2}$ and $C_l=C_0+\left(C_h-C_0\right)\frac{x}{\left(1-t\right)^2}$ are the temperature and the dilution at the upper plate, supposed to vary along the outward and in time, respectively.

The following dimensionless variables are used to make the conventional equations non-dimensional.

$$t=\overline{t}\frac{u_w}{h},\ x=\frac{\overline{x}}{h},y=\frac{\overline{y}}{h},u=\frac{\overline{u}}{u_w},v=\frac{\overline{v}}{u_w},p=\frac{\overline{p}}{p_0},\ T=\frac{\overline{T}-T_0}{T_h-T_0},C=\frac{\overline{C}-C_0}{C_h-C_0} \tag{9}$$

Then the dimensionless PDE model is specified by the following equations.

$$\frac{\partial u}{\partial t}+u\frac{\partial u}{\partial x}+v\frac{\partial u}{\partial y}+\frac{u_w\lambda_S}{h}\left(\frac{\partial^2 u}{\partial t^2}+2u\frac{\partial^2 u}{\partial t\partial x}+2v\frac{\partial^2 u}{\partial t\partial y}+u^2\frac{\partial^2 u}{\partial x^2}+v^2\frac{\partial^2 u}{\partial y^2}+2uv\frac{\partial^2 u}{\partial x\partial y}\right)$$
$$=-\frac{p_0}{{u_w}^2\rho}\frac{\partial \overline{p}}{\partial \overline{x}}+\frac{1}{\mathrm{Re}}\frac{\partial^2 \overline{u}}{\partial \overline{y}^2}-\frac{\sigma {B_0}^2 h}{\rho u_w}\left(u+\frac{u_w\lambda_S}{h}\left(\frac{\partial u}{\partial t}+v\frac{\partial u}{\partial y}\right)\right) \tag{10}$$

$$\frac{\partial T}{\partial t}+u\frac{\partial T}{\partial x}+v\frac{\partial T}{\partial y}$$
$$=\frac{1}{PrRe}\left(\frac{\partial^2 T}{\partial y^2}\right)+\frac{1}{Re}\left(Nb_x\frac{\partial T}{\partial y}\frac{\partial C}{\partial y}+Nt_x\left(\frac{\partial T}{\partial y}\right)^2\right)+\frac{Ec_x}{Re}\left(\frac{\partial u}{\partial y}\right)^2 \tag{11}$$

$$\frac{\partial C}{\partial t}+u\frac{\partial C}{\partial x}+v\frac{\partial C}{\partial y}=\frac{1}{ReLe}\frac{\partial^2 C}{\partial y^2}+\frac{Nt_x}{ReLeNb_x}\frac{\partial^2 T}{\partial y^2} \tag{12}$$

Let ψ be the stream function. Set $u=\frac{\partial \psi}{\partial y}$ and $v=-\frac{\partial \psi}{\partial x}$ in the above equations to get

$$\frac{\partial^2\psi}{\partial t\partial y}+\frac{\partial\psi}{\partial y}\frac{\partial^2\psi}{\partial x\partial y}-\frac{\partial\psi}{\partial x}\frac{\partial^2\psi}{\partial y^2}+\frac{u_w\lambda_S}{h}\left(\frac{\partial^3\psi}{\partial t^2\partial y}+2\frac{\partial\psi}{\partial y}\frac{\partial^3\psi}{\partial t\partial x\partial y}\right.$$
$$\left.-2\frac{\partial\psi}{\partial x}\frac{\partial^3\psi}{\partial t\partial y^2}+\left(\frac{\partial\psi}{\partial y}\right)^2\frac{\partial^3\psi}{\partial x^2\partial y}+\left(\frac{\partial\psi}{\partial x}\right)^2\frac{\partial^3\psi}{\partial y^3}-2\frac{\partial\psi}{\partial y}\frac{\partial\psi}{\partial x}\frac{\partial^3\psi}{\partial x\partial y^2}\right) \tag{13}$$
$$=-\frac{p_0}{u_w^2\rho}\frac{\partial p}{\partial x}+\frac{1}{Re}\frac{\partial^3\psi}{\partial y^3}-\frac{\sigma B^2 h}{\rho u_w}\left(\frac{\partial\psi}{\partial y}+\frac{u_w\lambda_S}{h}\left(\frac{\partial^2\psi}{\partial t\partial y}-\frac{\partial\psi}{\partial x}\frac{\partial^2\psi}{\partial y^2}\right)\right)$$

$$\frac{\partial T}{\partial t}+\frac{\partial\psi}{\partial y}\frac{\partial T}{\partial x}-\frac{\partial\psi}{\partial x}\frac{\partial T}{\partial y}$$
$$=\frac{1}{RePr}\left(\frac{\partial^2 T}{\partial y^2}\right)+\frac{1}{Re}\left(Nb_x\frac{\partial T}{\partial y}\frac{\partial C}{\partial y}+Nt_x\left(\frac{\partial T}{\partial y}\right)^2\right)+\frac{Ec_x}{Re}\left(\frac{\partial^2\psi}{\partial y^2}\right)^2 \tag{14}$$

$$\frac{\partial C}{\partial \overline{t}}+\frac{\partial\psi}{\partial y}\frac{\partial C}{\partial x}-\frac{\partial\psi}{\partial x}\frac{\partial C}{\partial y}=\frac{1}{ReLe}\frac{\partial^2 C}{\partial y^2}+\frac{Nt_x}{ReLeNb_x}\frac{\partial^2 T}{\partial y^2} \tag{15}$$

Dimensionless boundary conditions for prescribed surface temperature (PST) are

$$\left.\begin{array}{l}\frac{\partial\psi}{\partial y}=\gamma_h,\ \frac{\partial\psi}{\partial x}=-\frac{v_h}{u_w},\ T=\frac{x}{(1-t)^2},\ C=\frac{x}{(1-t)^2}\quad \text{at } y=\frac{l}{h}\\ u=0,\qquad v=0,\quad T=0,\quad C=0\qquad\qquad \text{at } y=0\end{array}\right\} \tag{16}$$

Here $Re=\frac{u_w h}{\nu}$ is the Reynolds number, $Pr=\frac{\nu\rho Cp}{\kappa}$ is the Prandtl number; $Ec_x=\frac{u_w^2}{C_p\left(T_h-T_0\right)}$ is the Eckert number; $Nb_x=\frac{\tau D_B\left(C_h-C_0\right)}{\nu}$ is the Brownian motion parameter; $Nt_x=\frac{\tau D_T\left(T_h-T_0\right)}{\nu T_a}$ is the thermophoresis parameter;

$Le = \frac{\nu}{D_B}$ is the Lewis number.

3. Method of Transformations

The prominence of similarity solutions in many areas of science and engineering is limitless. Looking for a universal symmetric approach that can be applied to specific mathematical models is obligatory. The Lie group transformation procedure is a sound technique for the theory of the continuous symmetry of numerical structures, which is immensely functional for various fields of modern mathematical physics. This analysis is anticipated to deliver a new methodology for investigating the continuous symmetries of model equations leading to heat transfer fluxes in elastico-viscous nanofluids. In the process, the Lie group theory trims down the number of independent parameters of the central PDEs reflected in the physical model. It also maintains the invariant structure of the model with the corresponding initial and boundary conditions. Because of the unsteady flow ($0 < t < 1$) in a channel, the following two-parameter linear groups of transformations are to be considered for the Lie group analysis [47]:

$$\begin{aligned}\Gamma:\ & \hat{t} = (1-t)e^{\alpha_1},\ \hat{x} = xe^{\beta_1},\ \hat{\psi} = \psi e^{\alpha_2}e^{\beta_2},\ \hat{y} = ye^{\alpha_3}e^{\beta_3},\ \hat{T} = Te^{\alpha_4}e^{\beta_4},\ \hat{C} = Ce^{\alpha_5}e^{\beta_5},\\ & \hat{p} = pe^{\alpha_6}e^{\beta_6},\ \hat{\lambda}_S = \lambda_S e^{\alpha_7}e^{\beta_7},\ \hat{B}_0 = B_0 e^{\alpha_8}e^{\beta_8},\ E\hat{c} = Ec_x e^{\alpha_9}e^{\beta_9},\ \hat{\gamma}_h = \gamma_h e^{\alpha_{10}}e^{\beta_{10}},\\ & \hat{v}_h = v_h e^{\alpha_{11}}e^{\beta_{11}},\ \hat{l} = le^{\alpha_{12}}e^{\beta_{12}},\ \hat{N}b = Nb_x e^{\alpha_{13}}e^{\beta_{13}},\ \hat{N}t = Nt_x e^{\alpha_{14}}e^{\beta_{14}},\\ & \hat{h}_f = \overline{h}_f e^{\alpha_{15}}e^{\beta_{15}},\ \hat{h}_f^* = \overline{h}_f^* e^{\alpha_{16}}e^{\beta_{16}}\end{aligned} \tag{17}$$

Here $\alpha_i, \beta_i\ (i = 1,2,\cdots,16)$ are the constants taken in such a way that the forms of the Equations (13)-(15) are invariant under the transformations connected given in the following relations

$$\begin{aligned}&\alpha_2 = -\frac{1}{2}\alpha_1, \alpha_3 = \frac{1}{2}\alpha_1, \alpha_4 = -2\alpha_1, \alpha_5 = -2\alpha_1, \alpha_6 = -2\alpha_1, \alpha_7 = \alpha_1, \alpha_8 = -\frac{1}{2}\alpha_1, \alpha_9 = 0,\\ &\alpha_{10} = -\alpha_1, \alpha_{11} = -\frac{1}{2}\alpha_1, \alpha_{12} = \frac{1}{2}\alpha_1, \alpha_{13} = 2\alpha_1, \alpha_{14} = 2\alpha_1, \alpha_{15} = -\frac{1}{2}\alpha_1, \alpha_{16} = -\frac{1}{2}\alpha_1\\ &\beta_2 = \beta_1,\ \beta_3 = 0,\ \beta_4 = \beta_1,\ \beta_5 = \beta_1,\ \beta_6 = 2\beta_1,\ \beta_7 = 0,\ \beta_8 = 0,\ \beta_9 = -\beta_1,\\ &\beta_{10} = \beta_1,\ \beta_{11} = 0,\ \beta_{12} = 0,\ \beta_{13} = -\beta_1,\ \beta_{14} = -\beta_1,\ \beta_{15} = 0,\ \beta_{16} = 0\end{aligned} \tag{18}$$

With these relationships of α_i, β_i Equation (17) turns into

$$\begin{aligned}\Gamma:\ & \hat{t} = (1-t)e^{\alpha_1},\ \hat{x} = xe^{\beta_1},\ \hat{\psi} = \psi e^{-\frac{1}{2}\alpha_1}e^{\beta_1},\ \hat{y} = ye^{\frac{1}{2}\alpha_1},\ \hat{T} = Te^{-2\alpha_1}e^{\beta_1},\ \hat{C} = Ce^{-2\alpha_1}e^{\beta_1},\\ & \hat{p} = e^{-2\alpha_1}e^{2\beta_1},\ \hat{\lambda} = \lambda e^{\alpha_1}e^0,\ \hat{B}_0 = B_0 e^{-\frac{1}{2}\alpha_1}e^0,\ E\hat{c} = Ec_x e^0 e^{-\beta_1},\ \hat{\gamma}_h = \gamma_h e^{-\alpha_1}e^{\beta_1},\\ & \hat{v}_h = v_h e^{-\frac{1}{2}\alpha_1}e^0,\ \hat{l} = le^{\frac{1}{2}\alpha_1}e^0,\ \hat{N}b = Nbe^{2\alpha_1}e^{-\beta_1},\ \hat{N}t = Nte^{2\alpha_1}e^{-\beta_1},\ \hat{h}_f = \overline{h}_f e^{-\frac{1}{2}\alpha_1},\\ & \hat{h}_f^* = \overline{h}_f^* e^{-\frac{1}{2}\alpha_1}\end{aligned} \tag{19}$$

From the absolute invariants, the similarity parameters are designated as

$$\eta = \frac{y}{\sqrt{1-t}}, \psi = \frac{x}{\sqrt{1-t}} f(\eta), p = \frac{x^2}{(1-t)^2} p_\eta, \lambda_S = (1-t)\lambda_0, B_0 = \frac{B}{\sqrt{1-t}},$$
$$Ec_x = x^{-1} Ec, T = \frac{x}{(1-t)^2}\theta(\eta), C = \frac{x}{(1-t)^2} F(\eta), \gamma_h = \frac{x}{1-t}\gamma, v_h = \frac{v_w}{\sqrt{1-t}},$$
$$l = \sqrt{1-t}h, Nb_x = \frac{(1-t)^2}{x} Nb, Nt_x = \frac{(1-t)^2}{x} Nt, \bar{h}_f = h_f (1-t)^{-\frac{1}{2}}, \bar{h}_f^* = h_f^* (1-t)^{-\frac{1}{2}} \quad (20)$$

Using the above similarity transformations in Equations (13)-(15), we obtain the following similarity equations,

$$\left(\frac{1}{Re} - \frac{\beta_S}{4}\left(\eta^2 - 4\eta f + 4f^2\right)\right) f^{iv} - \frac{1}{2}\left(\eta f''' + 3f'' + 2f' f'' - 2f f'''\right)$$
$$-\frac{\beta_S}{4}\left(9\eta f''' + 4\eta f''^2 - 16 f f''' + 8 f' f'' - 8 f f''^2 - 8 f'^2 f'' + 15 f''\right) \quad (21)$$
$$-M\left(f'' + \frac{\beta_S}{2}\left(\eta f''' + 3f'' - 2f f''' - 2f' f''\right)\right) = 0$$

$$\theta'' - PrRe\left(\frac{\eta}{2}\theta' + 2\theta + f'\theta - f\theta'\right) + Pr\left(Nb\theta' F' + Nt\theta'^2\right) + PrEc f''^2 = 0 \quad (22)$$

$$F'' - ReLe\left(\frac{\eta}{2}F' + 2F + f'F - fF'\right) + \frac{Nt}{Nb}\theta'' = 0 \quad (23)$$

And the transformed PST boundary conditions are

$$\left.\begin{array}{l} f' = \gamma,\ f = f_w,\ \theta = 1,\ F = 1 \quad \text{at } \eta = 1 \\ f' = 0,\ f = 0,\ \theta = 0,\ F = 0 \quad \text{at } \eta = 0 \end{array}\right\} \quad (24)$$

Following a similar procedure, the PCB boundary conditions take the form

$$\left.\begin{array}{l} f' = \gamma,\ f = f_w,\quad \theta = 1,\qquad F = 1 \qquad\quad \text{at } \eta = 1 \\ f' = 0,\ f = 0,\ \theta' = -Bi(1-\theta),\ F' = -Bi^*(1-F) \quad \text{at } \eta = 0 \end{array}\right\} \quad (25)$$

Here $\beta_S = \frac{u_w \lambda_S}{h}$ is the Deborah number; $M = \frac{B_0^2 \sigma h}{\rho u_w}$ is the Magnetic field parameter; γ is the stretching parameter; $f_w = \frac{v_w}{u_w}$ is the suction parameter; $Bi = \frac{h_f h}{\kappa}$ and $Bi^* = \frac{h_f^* h}{\kappa}$ are the Biot numbers for convective heat and mass transfer, respectively.

Finally, the skin friction coefficient estimates the friction force functional to the surface, and the Nusselt number characterises the heat flux from a heated surface to a fluid. The skin friction coefficient (C_f), the local Nusselt number (Nu), and mass transfer (Sh) are defined as

$$C_f \propto f'', \quad Nu \propto \theta', \quad Sh \propto F' \quad (26)$$

4. Numerical Methods

The fourth-order collocation approach based on cubic polynomials is used by the

bvp4c package, which offers a fair trade-off between computing cost and accuracy. It is appropriate for a variety of engineering challenges due to its ability to efficiently solve nonlinear differential equations and nonlinear boundary conditions. One of its important characteristics is automated mesh adaptation, which maintains accuracy without needless processing by fine-tuning the solution grid where necessary. *bvp4c*, which is integrated into MATLAB, features an easy-to-use interface and supports multipoint boundary conditions, vectorised formulations, and parameter continuation. *bvp4c* is dependable and quick for issues with a moderate number of differential equations.

For boundary value issues requiring convective or specified temperature boundary conditions in heat transfer, *bvp4c* and its Collocation Method are perfect. It can be used to represent issues with elastic stability, vibration, and beam deflection. It is also employed to address flow in porous media and laminar boundary layer issues. Modelling thermal profiles in engine parts, brake systems, or even battery thermal management is one of the main applications for this technique.

Equations (21)-(23) combined with the boundary conditions Equation (24) and Equation (25) individually are solved numerically using the collocation method developed by a MATLAB package, known as *bvp4c*. The analysis is made for various parameters like Deborah number or Maxwell parameter (β_S), stretching parameter (γ), suction parameter (f_w), magnetic field parameter (M), Prandtl number (Pr), Eckert number (Ec), thermophoresis parameter (Nt), Brownian motion parameter (Nb), and Lewis number (Le). The mesh size is $\eta = 0.01$, and the tolerance factor is set 10^{-6}. Based on the contemporary model, [0, 1] is considered the channel problem domain.

5. Results and Discussion

The renovation of the model equations trims down the mathematical work extensively. Graphical representations of consequences are very constructive in discussing the physical features offered by the solutions.

In nanofluid systems, the Brownian diffusion of particles is an essential factor in studying the nanoparticle effects on the flow field, temperature and nanoparticle volume fraction (NVF) distributions since the particle size approaches the nanometer scale. Brownian diffusion is accompanied by the arbitrary motion of particles suspended in a conventional fluid after collision with the molecules of the base fluid, which is an imperative mechanism to improve heat transmission. **Figure 2** and **Figure 3** illustrate the impact of Brownian motion parameter on thermal and mass boundary layers, respectively, for both cases: PST (solid line) and PCB (dashed line). From **Figure 2**, it is noticed that the temperature distribution enhances as *Nb* improves in both cases. The higher Brownian motion parameter yields enhanced diffusion; that's why the collision of particles increases. So, the temperature is raised after collation and produces an augmented thermal boundary layer; an analogous conclusion was expressed by Khan and Pop [48] in their work.

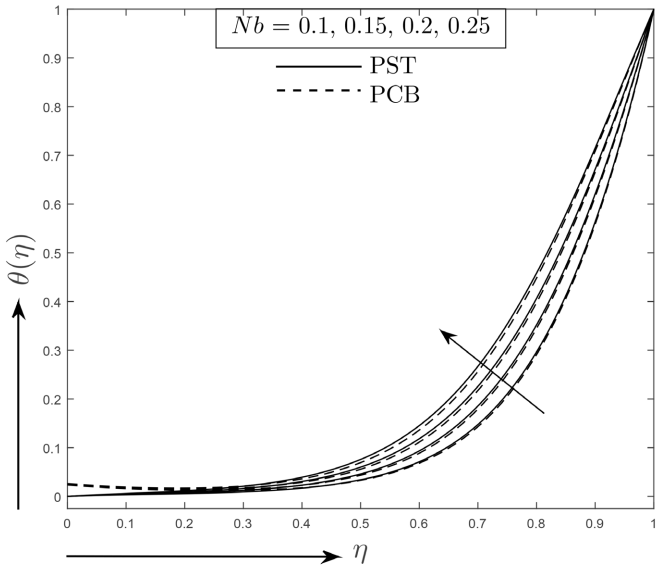

Figure 2. Temperature distribution for the Brownian motion parameter *Nb*.

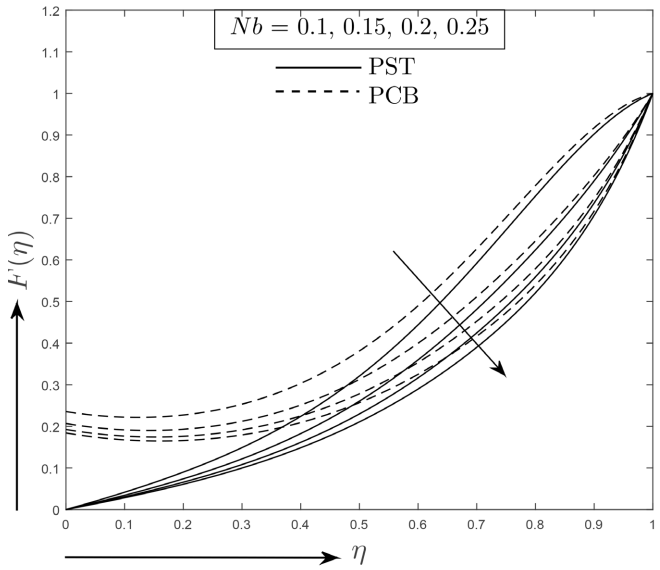

Figure 3. Volume fraction distribution for the Brownian motion parameter *Nb*.

Figure 3 demonstrates that the NVF initially increases for higher *Nb* near the lower wall. But apart from the lower wall after $\eta = 0.22$, those profiles reverse the trend and begin to fall due to growing *Nb* for the PST state. Again, as the Brownian motion parameter is higher, the NVF reduces throughout the flow regime for the PCB boundary condition; a parallel discussion is ended by Aziz and Khan [49].

Thermophoresis diffusion occurs due to a temperature gradient force, for which the nanoparticles in the mixture reveal dissimilar reactions. The local temperature in the thermal boundary layer improves laterally with the liquid flow re-

gime since the thermophoresis parameter *Nt* increases, as revealed in Figure 4, for both PST (continuous line) and PCB (discontinuous line) boundary conditions. Eldabe and Abou-zeid [50] discovered a similar result in 2017. Figure 5 indicates that the NVF profile raises for higher thermophoresis parameter *Nt* throughout the flow system for PCB boundary conditions (dashed line). But the distribution of NVF decreases in the domain $\eta \in [0, 0.23]$ and increases in the remaining regime for higher *Nt* for PST boundary conditions (solid line).

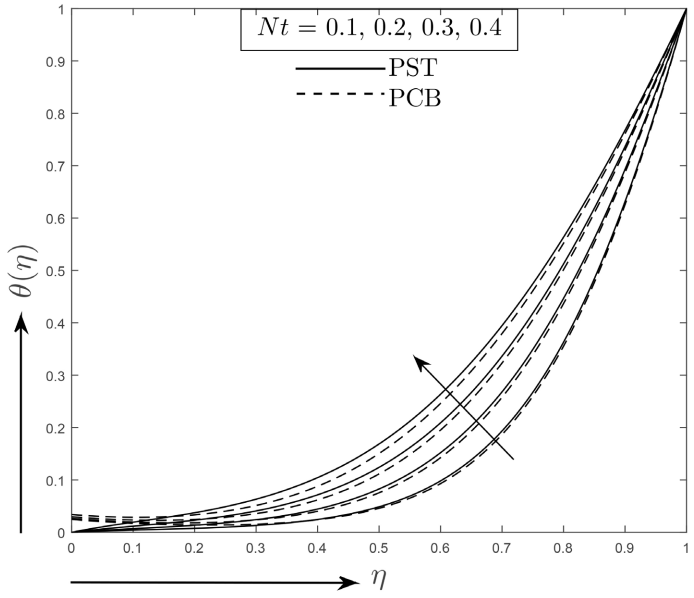

Figure 4. Temperature distribution for the thermophoresis parameter *Nt*.

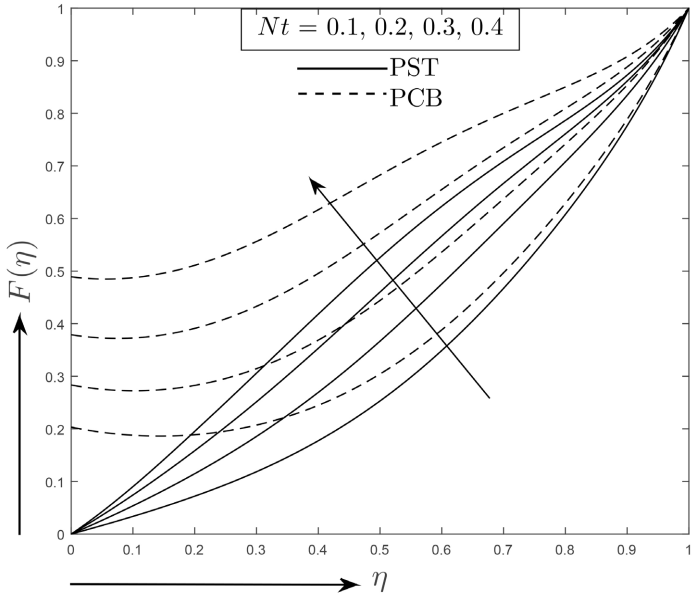

Figure 5. Volume fraction distribution for the thermophoresis parameter *Nt*.

The Eckert (*Ec*) number states the affiliation of kinetic energy and the enthalpy variance of the boundary layer in a fluid flow. A considerable Eckert number produces an escalation in the kinetic energy of nanofluid particles. Accordingly, the fluid heats up, and the temperature rises. Figure 6 illustrates that the Eckert number develops the heat transportation in the liquid, which is a vital tool for the advancement of energy transference in nanofluids, in accordance with Atif *et al.* [51]. Figure 7 indicates the NVF profile dropping for higher Eckert numbers over the PST boundary condition flow system (solid line). But the outline of the nanoparticles volume fraction escalates in the domain $\eta \in [0.341, 0.718]$ and declines in the remaining regime for higher *Ec* for PCB boundary conditions (dashed line).

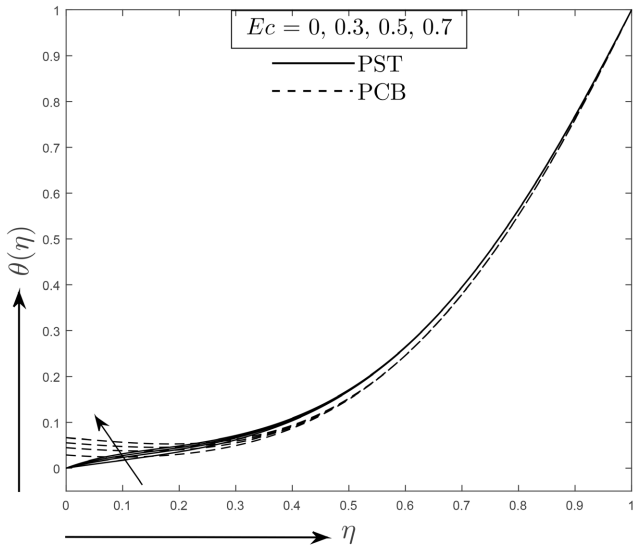

Figure 6. Temperature distribution for the thermophoresis parameter *Ec*.

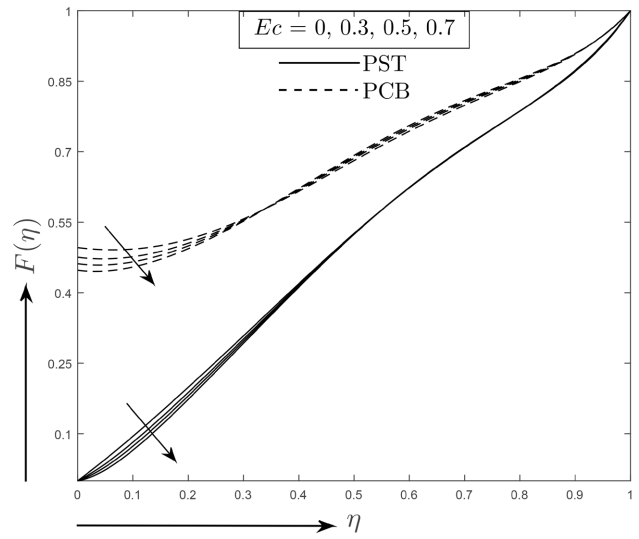

Figure 7. Volume fraction distribution for the thermophoresis parameter *Ec*.

The Deborah number (β_S) is a dimensionless variable that treats the fluid relaxation time to its characteristic time scale. Here $\beta_S = 0$ gives the incompressible Newtonian fluid feature. Liquids with a small Deborah number have a liquid-like behaviour, while a large Deborah number communicates that solids-like substances can better conduct and retain heat. Therefore, it is witnessed that regularly increasing the Deborah number boosts the fluid viscosity, which increases the confrontation in momentum. Consequently, the hydrodynamic boundary layer thickness reduces because of the Maxwell fluid, as revealed in Figure 8, leading to a good connection with Bilal *et al.* [52]. No deviation is created for different boundary conditions. An exciting fact, i.e., a crosswise flow occurs here between $\eta = 0.22$ and $\eta = 0.71$.

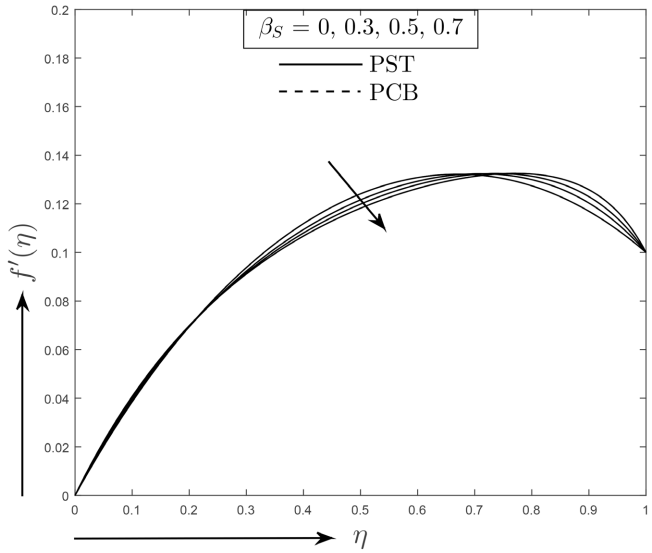

Figure 8. Momentum distribution for the Deborah number β_S.

Figures 9-11 represent the consequences of suction (f_w) on momentum, thermal, and NVF distributions, respectively. It is particularly from these figures that momentum and thermal distributions are increasing due to higher suction for both the PST and PCB boundary surfaces. Physically, the imposed suction brings a force to the liquid in the waterway, improving the fluid's movement and energy. In addition, the NVF profile declines with the more incredible suction.

From Figure 12, it is discovered that the wall stretching factor enhances the fluid velocity to increase the momentum distribution with the stretching effect (γ) growth nearby the upper wall, where the momentum distribution is reduced within the flow regime $\eta \in [0, 0.732]$. As a result, across-flow occurs.

The magnetic field parameter (M) effects on momentum are demonstrated in Figure 13 for both instances. It is developed from the magnetic field strength imposed on an electrically conductive fluid, which generates a drag force called the Lorentz force against the flow direction along the surface to slow down the velocity. It is perceived that a rise in the magnetic field parameter values monotonically

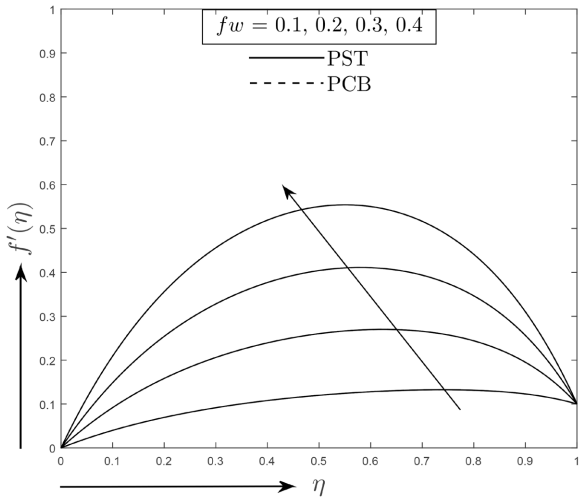

Figure 9. Velocity distribution for the suction parameter f_w.

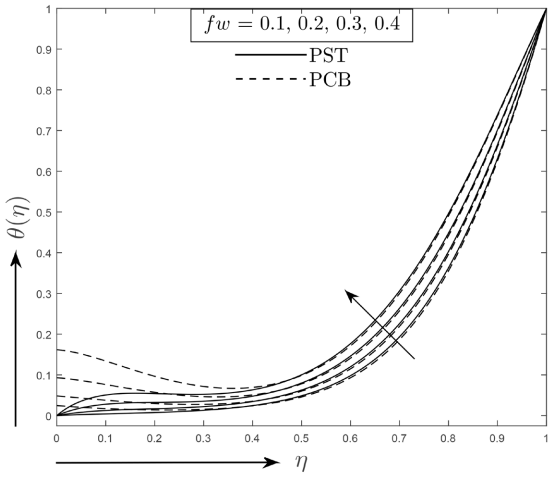

Figure 10. Temperature distribution for the suction parameter f_w.

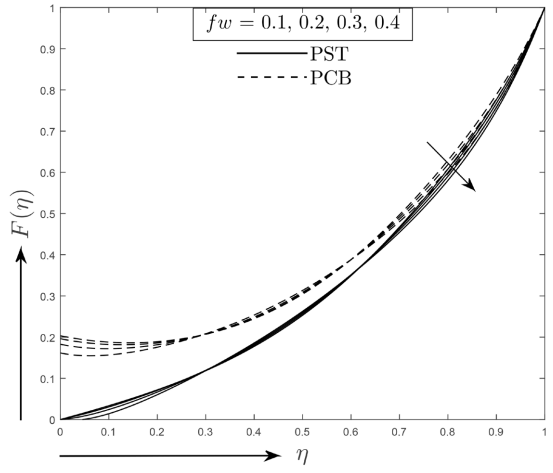

Figure 11. Volume fraction distribution for the suction parameter f_w.

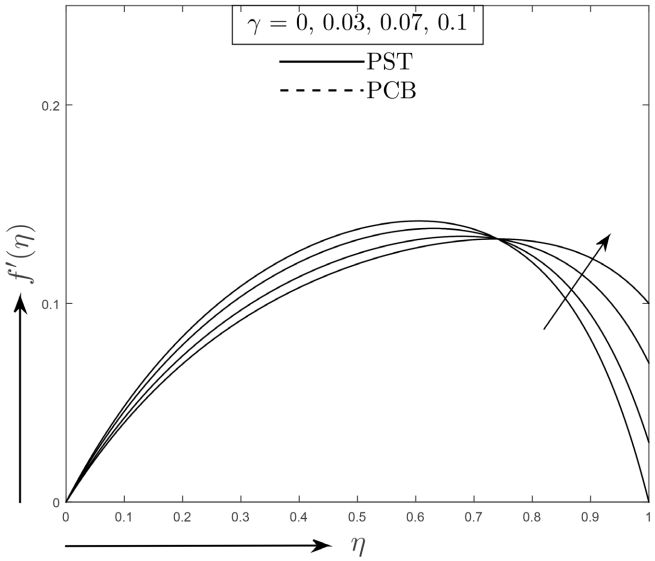

Figure 12. Momentum distribution for the stretching parameter γ.

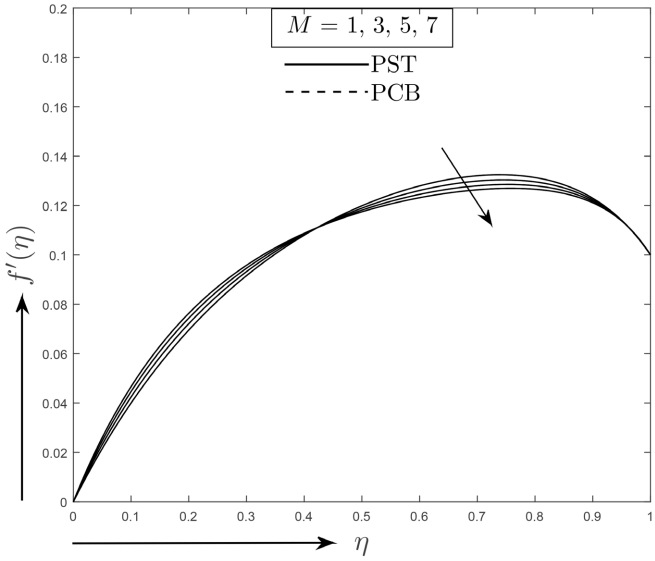

Figure 13. Momentum distribution for the magnetic parameter *M*.

reduces the momentum distribution. That is why the imposed magnetic field is responsible for smoothing the fluid flow velocity. Finally, also crosswise flow exists for magnetic field parameter variation.

Additionally, the effect of the stress relaxation parameter on the skin fraction coefficient (f''), the local Nusselt number ($-\theta'$) and the Sherwood number ($-F'$) are arranged in Table 1 for PST and Table 2 for PCB, considering $Re = 1$, $M = 1$, $Pr = 21$, $Ec = 0.1$, $Le = 5$, $Nb = 0.16$, $Nt = 0.1$, $\gamma = 0.1$, $f_w = 0.1$, $Bi = 0.1$ and $Bi^* = 0.3$.

Heat Transfer Rate for Brownian Motion Parameter

Figure 14 is prepared to portray the consequence of the Brownian motion parameter (*Nb*) on the Nusselt number (*Nu*) at the lower wall $\eta = 0$ for the

Deborah number (β_S) for PST and PCB. It is noticeable from these figures that the heat transmission rate decays for the progressive values of the Brownian motion parameter (*Nb*) as the Deborah number increases. Figure 15 is arranged to define the control of the Brownian motion parameter on the Nusselt number at the upper surface $\eta = 1$ over the Deborah number for PST and PCB. It is visible from these figures that the energy transfer rate (*Nu*) is enhanced for the more significant Brownian motion parameter as the Deborah number develops.

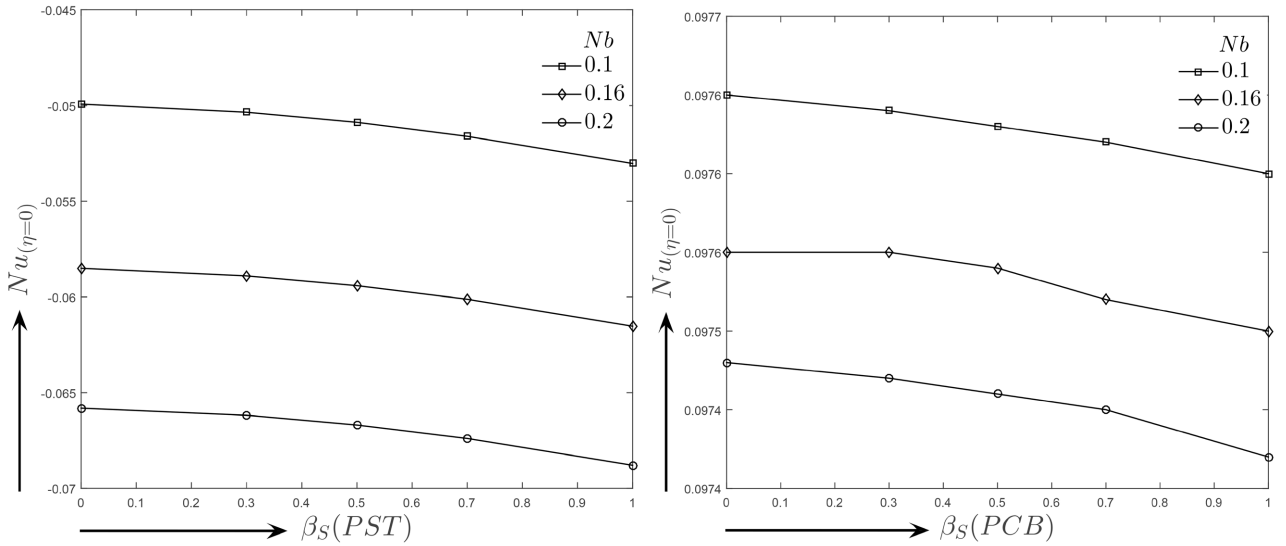

Figure 14. Nusselt number (*Nu*) distribution for the Brownian motion parameter (*Nb*) over the Deborah number (β_S) at the lower plate $\eta = 0$.

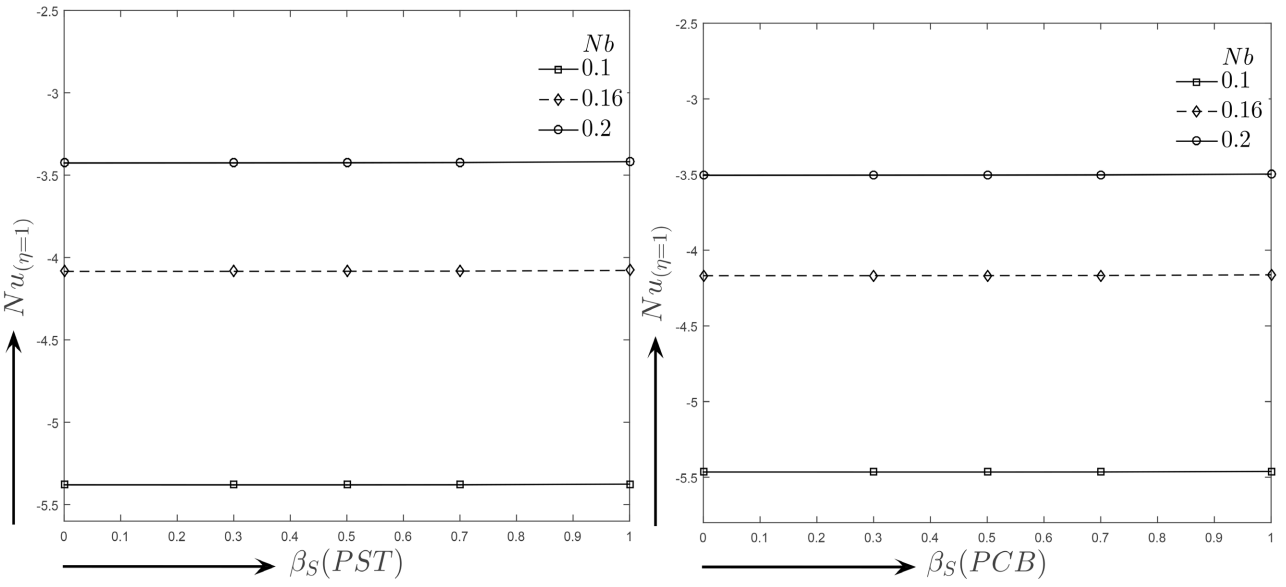

Figure 15. Nusselt number (*Nu*) distribution for the Brownian motion parameter (*Nb*) over the Deborah number (β_S) at the upper plate $\eta = 1$.

Table 1 is tabulated to investigate the mathematical computations of friction drag coefficient f'', heat transfer ($-\theta''$), and mass transfer ($-F'$) using dissimilar values of Deborah number (β_S) for PST conditions at the lower ($\eta = 0$) and upper ($\eta = 1$) plates, respectively. The local skin-friction factor increases with the lessening of the boundary layer. At the lower plate ($\eta = 0$), the friction drag and mass transfer rate escalate because of the greater Deborah number, while the heat transmission rate decreases. However, an opposite approach is seen at the upper plate ($\eta = 1$).

Table 2 describes the numerical estimations of friction drag coefficient, heat and mass transmission rates using the Deborah number for prescribed convective boundary (PCB) conditions at the lower ($\eta = 0$) and upper ($\eta = 1$) plates, respectively.

Table 1. Skin Friction (C_f), heat transfer (Nu), and mass transfer (Sh) for different values of Deborah number (β_S) for PST condition.

β_S	lower plate $\eta = 0$			upper plate $\eta = 1$		
	C_f	Nu	Sh	C_f	Nu	Sh
0	2.941705	−1.873448	2.414107	−2.705177	−1.206194	−3.59241
0.5	3.252821	−1.902969	2.527335	−3.135966	−1.110242	−3.86481
1	3.540485	−1.946570	2.663467	−3.527103	−1.020276	−4.11401
1.5	3.806786	−1.997095	2.809007	−3.889995	−0.934848	−4.34638
2	4.054486	−2.050718	2.957048	−4.231886	−0.852900	−4.56619

Table 2. Skin Friction (C_f), heat transfer (Nu), and mass transfer (Sh) for different values of Deborah number (β_S) for PCB condition.

β_S	lower plate $\eta = 0$			upper plate $\eta = 1$		
	C_f	Nu	Sh	C_f	Nu	Sh
0	2.941705	0.060429	0.251017	−2.705177	−1.256383	−3.226354
0.5	3.252821	0.059256	0.258964	−3.135966	−1.161220	−3.492534
1	3.540485	0.057867	0.266926	−3.527103	−1.072255	−3.733773
1.5	3.806786	0.056386	0.274675	−3.889995	−0.987933	−3.957295
2	4.054486	0.054879	0.282124	−4.231886	−0.907137	−4.167871

6. Conclusions

In automobile engineering, accurate thermal analysis is critical for ensuring the performance, safety, and longevity of various components. Two important thermal boundary conditions often applied in simulations and experimental setups are PST and PCB conditions. These conditions represent controlled thermal environments that allow engineers to analyse heat transfer behaviour under specific scenarios. PST condition is particularly useful when studying systems like engine blocks, exhaust manifolds, or battery packs, where surface temperature data can

be measured or estimated reliably. PCB condition, on the other hand, is appropriate for simulating and designing effective thermal management systems that require more realistic interactions between solid components and cooling medium, such as air or coolant, which are reflected in these boundary conditions.

The following is a summary of the important implications derived from the report of the current model.

- The thermal profile is improved for Brownian motion, thermophoresis, Eckert number, and suction parameters for PST and PCB.
- The Deborah number and magnetic parameter dominate the hydrodynamic boundary layer thickness for both PST and PCB conditions.
- It is essential to regulate the impact of the stretching feature of a wall to improve heat transmission with controlled fluid velocity.
- The advanced Deborah number is accountable for the developed shearing stress.

In conclusion, this research asserts that the model demonstrates velocity control phenomena and enhances heat transfer in nanofluids, presenting a significant possibility to enhance the cooling efficiency of mechanical systems with reduced friction.

Conflicts of Interest

The authors declare no conflicts of interest regarding the publication of this paper.

References

[1] Choi, S.U. and Eastman, J.A. (1995) Enhancing Thermal Conductivity of Fluids with Nanoparticles. Argonne National Lab., IL (United States).

[2] Wen, D. and Ding, Y. (2005) Formulation of Nanofluids for Natural Convective Heat Transfer Applications. *International Journal of Heat and Fluid Flow*, **26**, 855-864. https://doi.org/10.1016/j.ijheatfluidflow.2005.10.005

[3] Choi, S.U.S. (2009) Nanofluids: From Vision to Reality through Research. *Journal of Heat Transfer*, **131**, Article 033106. https://doi.org/10.1115/1.3056479

[4] Wong, K.V. and De Leon, O. (2010) Applications of Nanofluids: Current and Future. *Advances in Mechanical Engineering*, **2**, Article 519659. https://doi.org/10.1155/2010/519659

[5] Mahian, O., Kianifar, A., Kalogirou, S.A., Pop, I. and Wongwises, S. (2013) A Review of the Applications of Nanofluids in Solar Energy. *International Journal of Heat and Mass Transfer*, **57**, 582-594. https://doi.org/10.1016/j.ijheatmasstransfer.2012.10.037

[6] Taylor, R., Coulombe, S., Otanicar, T., Phelan, P., Gunawan, A., Lv, W., *et al.* (2013) Small Particles, Big Impacts: A Review of the Diverse Applications of Nanofluids. *Journal of Applied Physics*, **113**, Article 011301. https://doi.org/10.1063/1.4754271

[7] Uddin, M., Al Kalbani, K.S., Rahman, M., Alam, M., Al-Salti, N. and Eltayeb, I. (2016) Fundamentals of Nanofluids: Evolution, Applications and New Theory. *International Journal of Biomathematics Systems Biology*, **2**, 1-32.

[8] Zhou, S., Bilal, M., Khan, M.A. and Muhammad, T. (2021) Numerical Analysis of Thermal Radiative Maxwell Nanofluid Flow Over-Stretching Porous Rotating Disk. *Micromachines*, **12**, Article 540. https://doi.org/10.3390/mi12050540

[9] Buongiorno, J. (2005) Convective Transport in Nanofluids. *Journal of Heat Transfer*, **128**, 240-250. https://doi.org/10.1115/1.2150834

[10] Zangooee, M.R., Hosseini, S.A. and Ganji, D.D. (2020) Squeezing Nanofluid Flow between Parallel Rotating Plates Analysis by AGM Method. *International Journal of Ambient Energy*, **43**, 3322-3329. https://doi.org/10.1080/01430750.2020.1824945

[11] Seadawy, A., Raza, N., Khalil, O.H., Khan, K.A. and Usman, M. (2021) Computational Approach and Flow Analysis of Chemically Reactive Tangent Hyperbolic Nanofluid over a Cone and Plate. *Waves in Random and Complex Media*, **34**, 2540-2554. https://doi.org/10.1080/17455030.2021.1959960

[12] Rashidi, M.M., Akolade, M.T., Awad, M.M., Ajibade, A.O. and Rashidi, I. (2021) Second Law Analysis of Magnetized Casson Nanofluid Flow in Squeezing Geometry with Porous Medium and Thermophysical Influence. *Journal of Taibah University for Science*, **15**, 1013-1026. https://doi.org/10.1080/16583655.2021.2014691

[13] Makinde, O. and Mhone, P. (2005) Heat Transfer to MHD Oscillatory Flow in a Channel Filled with Porous Medium. *Romanian Journal of Physics*, **50**, 931-938.

[14] Sheikholeslami, M. and Ganji, D. (2014) Magnetohydrodynamic Flow in a Permeable Channel Filled with Nanofluid. *Scientia Iranica. Transaction B, Mechanical Engineering*, **21**, 203-212.

[15] Abbas, Z., Sajid, M. and Hayat, T. (2006) MHD Boundary-Layer Flow of an Upper-Convected Maxwell Fluid in a Porous Channel. *Theoretical and Computational Fluid Dynamics*, **20**, 229-238. https://doi.org/10.1007/s00162-006-0025-y

[16] Ramos, J.I. and Winowich, N.S. (1986) Magnetohydrodynamic Channel Flow Study. *The Physics of Fluids*, **29**, 992-997. https://doi.org/10.1063/1.865695

[17] Belhocine, A., Stojanovic, N. and Abdullah, O.I. (2021) Numerical Simulation of Laminar Boundary Layer Flow over a Horizontal Flat Plate in External Incompressible Viscous Fluid. *European Journal of Computational Mechanics*, **30**, 337-386. https://doi.org/10.13052/ejcm2642-2085.30463

[18] Pavar, P., Harikrishna, L. and Reddy, M.S. (2021) Heat Transfer over a Stretching Porous Surface on a Steady MHD Fluid Flow. *International Journal of Ambient Energy*, **43**, 4398-4405. https://doi.org/10.1080/01430750.2020.1848915

[19] Li, Y., Ullah, I., Ameer Ahammad, N., Ullah, I., Muhammad, T. and Asiri, S.A. (2022) Approximation of Unsteady Squeezing Flow through Porous Space with Slip Effect: DJM Approach. *Waves in Random and Complex Media*, **35**, 2679-2693. https://doi.org/10.1080/17455030.2022.2046298

[20] Harris, J. (1977) Rheology and Non-Newtonian Flow. Longman Publishing Group.

[21] Cameron, A. and Mc Ettles, C. (1981) Basic Lubrication Theory. Ellis Horwood.

[22] Barnes, H.A., Hutton, J.F. and Walters, K. (1989) An Introduction to Rheology. Elsevier.

[23] Olsson, F. and Yström, J. (1993) Some Properties of the Upper Convected Maxwell Model for Viscoelastic Fluid Flow. *Journal of Non-Newtonian Fluid Mechanics*, **48**, 125-145. https://doi.org/10.1016/0377-0257(93)80068-m

[24] Sochi, T. (2010) Flow of Non-Newtonian Fluids in Porous Media. *Journal of Polymer Science Part B: Polymer Physics*, **48**, 2437-2767. https://doi.org/10.1002/polb.22144

[25] Udupa, M., Shankar Narayan, S. and Saha, S. (2020) A Study of the Blood Flow Using Newtonian and Non-Newtonian Approach in a Stenosed Artery. In: Singh, P., Gupta, R.K., Ray, K. and Bandyopadhyay, A., Eds., *Proceedings of International Conference on Trends in Computational and Cognitive Engineering*, Springer, 257-269. https://doi.org/10.1007/978-981-15-5414-8_21

[26] Li, X.K., Luo, Y., Qi, Y. and Zhang, R. (2011) On Non-Newtonian Lubrication with the Upper Convected Maxwell Model. *Applied Mathematical Modelling*, **35**, 2309-2323. https://doi.org/10.1016/j.apm.2010.11.003

[27] Fetecau, C. and Fetecau, C. (2003) A New Exact Solution for the Flow of a Maxwell Fluid Past an Infinite Plate. *International Journal of Non-Linear Mechanics*, **38**, 423-427. https://doi.org/10.1016/s0020-7462(01)00062-2

[28] Mustafa, M., Khan, J.A., Hayat, T. and Alsaedi, A. (2015) Simulations for Maxwell Fluid Flow Past a Convectively Heated Exponentially Stretching Sheet with Nanoparticles. *AIP Advances*, **5**, Article 037133. https://doi.org/10.1063/1.4916364

[29] Habib, U., Abdal, S., Siddique, I. and Ali, R. (2021) A Comparative Study on Micropolar, Williamson, Maxwell Nanofluids Flow Due to a Stretching Surface in the Presence of Bioconvection, Double Diffusion and Activation Energy. *International Communications in Heat and Mass Transfer*, **127**, Article 105551. https://doi.org/10.1016/j.icheatmasstransfer.2021.105551

[30] Jamshed, W., Eid, M.R., Aissa, A., Mourad, A., Nisar, K.S., Shahzad, F., *et al.* (2021) Partial Velocity Slip Effect on Working Magneto Non-Newtonian Nanofluids Flow in Solar Collectors Subject to Change Viscosity and Thermal Conductivity with Temperature. *PLOS ONE*, **16**, e0259881. https://doi.org/10.1371/journal.pone.0259881

[31] Machireddy, G.R., Praveena, M.M., Rudraswamy, N.G. and Kumar, G.K. (2021) Impact of Cattaneo-Christov Heat Flux on Hydromagnetic Flow of Non-Newtonian Fluids Filled with Darcy-Forchheimer Porous Medium. *Waves in Random and Complex Media*, **34**, 2425-2442. https://doi.org/10.1080/17455030.2021.1957178

[32] Subhas Abel, M., Tawade, J.V. and Nandeppanavar, M.M. (2012) MHD Flow and Heat Transfer for the Upper-Convected Maxwell Fluid over a Stretching Sheet. *Meccanica*, **47**, 385-393. https://doi.org/10.1007/s11012-011-9448-7

[33] Omowaye, A.J. and Animasaun, I.L. (2016) Upper-Convected Maxwell Fluid Flow with Variable Thermo-Physical Properties over a Melting Surface Situated in Hot Environment Subject to Thermal Stratification. *Journal of Applied Fluid Mechanics*, **9**, 1777-1790. https://doi.org/10.18869/acadpub.jafm.68.235.24939

[34] Fetecau, C., Vieru, D., Abbas, T. and Ellahi, R. (2021) Analytical Solutions of Upper Convected Maxwell Fluid with Exponential Dependence of Viscosity under the Influence of Pressure. *Mathematics*, **9**, Article 334. https://doi.org/10.3390/math9040334

[35] Waqas, H., Manzoor, U., Hussain, S. and Bhatti, M.M. (2021) Maxwell Time-Dependent Nanofluid Flow over a Wedge Covered with Gyrotactic Microorganism: An Activation Energy Process. *International Journal of Ambient Energy*, **43**, 5560-5570. https://doi.org/10.1080/01430750.2021.1969274

[36] Khan, S.U., Usman, Al-Khaled, K., Hussain, S.M., Ghaffari, A., Khan, M.I., *et al.* (2022) Implication of Arrhenius Activation Energy and Temperature-Dependent Viscosity on Non-Newtonian Nanomaterial Bio-Convective Flow with Partial Slip. *Arabian Journal for Science and Engineering*, **47**, 7559-7570. https://doi.org/10.1007/s13369-021-06274-3

[37] Levi, D., Vinet, L. and Winternitz, P. (1997) Lie Group Formalism for Difference Equations. *Journal of Physics A*: *Mathematical and General*, **30**, 633-649. https://doi.org/10.1088/0305-4470/30/2/024

[38] Yürüsoy, M. and Pakdemirli, M. (1997) Symmetry Reductions of Unsteady Three-Dimensional Boundary Layers of Some Non-Newtonian Fluids. *International Journal of Engineering Science*, **35**, 731-740. https://doi.org/10.1016/s0020-7225(96)00115-2

[39] Ibragimov, N.K. and Ibragimov, N.K. (1999) Elementary Lie Group Analysis and Ordinary Differential Equations. Vol. 197, Wiley.

[40] Rosmila, A.B., Kandasamy, R. and Muhaimin, I. (2012) Lie Symmetry Group Transformation for MHD Natural Convection Flow of Nanofluid over Linearly Porous Stretching Sheet in Presence of Thermal Stratification. *Applied Mathematics and Mechanics*, **33**, 593-604. https://doi.org/10.1007/s10483-012-1573-9

[41] Ovsiannikov, L.V.E. (2014) Group Analysis of Differential Equations. Academic Press.

[42] Saleem, M., Tufail, M.N. and Chaudhry, Q.A. (2022) Significance of the Physical Quantities for the Non-Newtonian Fluid Flow in an Irregular Channel with Heat and Mass Transfer Effects: Lie Group Analysis. *Alexandria Engineering Journal*, **61**, 1968-1980. https://doi.org/10.1016/j.aej.2021.07.003

[43] Uddin, M.J., Kabir, M.N. and Alginahi, Y.M. (2015) Lie Group Analysis and Numerical Solution of Magnetohydrodynamic Free Convective Slip Flow of Micropolar Fluid over a Moving Plate with Heat Transfer. *Computers & Mathematics with Applications*, **70**, 846-856. https://doi.org/10.1016/j.camwa.2015.06.002

[44] Ahmad, S., Diyar, R. and Zeb, S. (2021) Lie Group Analysis of Hyperbolic Tangent Fluid Flow in the Presence of Thermal Radiation. *Heat Transfer*, **51**, 3067-3081. https://doi.org/10.1002/htj.22437

[45] Bhatti, M.M., Jun, S., Khalique, C.M., Shahid, A., Fasheng, L. and Mohamed, M.S. (2022) Lie Group Analysis and Robust Computational Approach to Examine Mass Transport Process Using Jeffrey Fluid Model. *Applied Mathematics and Computation*, **421**, Article 126936. https://doi.org/10.1016/j.amc.2022.126936

[46] Kuznetsov, A.V. and Nield, D.A. (2010) Natural Convective Boundary-Layer Flow of a Nanofluid Past a Vertical Plate. *International Journal of Thermal Sciences*, **49**, 243-247. https://doi.org/10.1016/j.ijthermalsci.2009.07.015

[47] Uddin, M.J., Rashidi, M.M., Alsulami, H.H., Abbasbandy, S. and Freidoonimeh, N. (2016) Two Parameters Lie Group Analysis and Numerical Solution of Unsteady Free Convective Flow of Non-Newtonian Fluid. *Alexandria Engineering Journal*, **55**, 2299-2308. https://doi.org/10.1016/j.aej.2016.05.009

[48] Khan, W.A. and Pop, I. (2010) Boundary-Layer Flow of a Nanofluid Past a Stretching Sheet. *International Journal of Heat and Mass Transfer*, **53**, 2477-2483. https://doi.org/10.1016/j.ijheatmasstransfer.2010.01.032

[49] Aziz, A. and Khan, W.A. (2012) Natural Convective Boundary Layer Flow of a Nanofluid Past a Convectively Heated Vertical Plate. *International Journal of Thermal Sciences*, **52**, 83-90. https://doi.org/10.1016/j.ijthermalsci.2011.10.001

[50] Eldabe, N.T. and Abou-zeid, M.Y. (2017) Homotopy Perturbation Method for MHD Pulsatile Non-Newtonian Nanofluid Flow with Heat Transfer through a Non-Darcy Porous Medium. *Journal of the Egyptian Mathematical Society*, **25**, 375-381. https://doi.org/10.1016/j.joems.2017.05.003

[51] Atif, S.M., Hussain, S. and Sagheer, M. (2019) Effect of Viscous Dissipation and Joule Heating on MHD Radiative Tangent Hyperbolic Nanofluid with Convective and Slip Conditions. *Journal of the Brazilian Society of Mechanical Sciences and Engineering*, **41**, Article No. 189. https://doi.org/10.1007/s40430-019-1688-9

[52] Bilal, M., Sagheer, M. and Hussain, S. (2018) Three Dimensional MHD Upper-Convected Maxwell Nanofluid Flow with Nonlinear Radiative Heat Flux. *Alexandria Engineering Journal*, **57**, 1917-1925. https://doi.org/10.1016/j.aej.2017.03.039